Optical clearing of unsectioned specimens for three-dimensional imaging via optical transmission and emission tomography

Mark Oldham
Harshad Sakhalkar
Duke University Medical Center
Department of Radiation Oncology
Durham, North Carolina 27710

Tim Oliver
Duke University Medical Center
Department of Cell Biology
Durham, North Carolina 27710

G. Allan Johnson
Duke University Medical Center
Department of Radiology
Durham, North Carolina 27710

Mark Dewhirst
Duke University Medical Center
Department of Radiation Oncology
Durham, North Carolina 27710

Abstract. Optical computed tomography (optical-CT) and optical emission computed tomography (optical-ECT) are new techniques that enable unprecedented high-resolution 3-D multimodal imaging of tissue structure and function. Applications include imaging macroscopic gene expression and microvasculature structure in unsectioned biological specimens up to 8 cm^3. A key requisite for these imaging techniques is effective sample preparation including optical clearing, which enables light transport through the sample while preserving the signal (either light absorbing stain or fluorescent proteins) in representative form. We review recent developments in optical-CT and optical-ECT, and compatible "fluorescence-friendly" optical clearing protocols.
[DOI: 10.1117/1.2907968]

Keywords: optical; clearing; imaging; 3D; emission; tomography; gene; expression; vasculature; HIF1; xenograft.

Paper 07285SSR received Jul. 27, 2007; revised manuscript received Nov. 15, 2007; accepted for publication Dec. 14, 2007; published online Apr. 29, 2008.

1 Introduction

The ability to image co-registered biological structure and function in three dimensions in whole unsectioned tissue specimens is of significant present interest. In cancer research, for example, new antiangiogenic agents have potential to enhance the therapeutic effects of principal cancer treatments such as radiation and chemotherapy.[1,2] There is a need for greater understanding of the complex relationships governing the response of the global microvasculature to these agents to help development of more effective therapies.[3–5] These efforts have been hampered by the lack of a truly 3-D imaging modality with sufficiently high spatial resolution and contrast to determine subtle microvasculature detail. Such a modality would facilitate study of the vascular response to new therapeutic agents, to variations in fractionation of application,[6,7] the restructuring of vasculature networks,[8] and the distribution of functional response to hypoxia.[9,10] Imaging fine microvascular structure presents a challenge to existing imaging techniques, including micro-CT (micro-computed tomography) and micro-MRI (micro-magnetic resonance imaging) due to the combined requirement for high contrast and high spatial resolution. Similarly, there is great interest in techniques that can image the efficacy of drug and gene delivery techniques, gene expression, and the genetic response of tumors to therapy.[11–14] Optical responses to these challenges are now feasible with the development of fluorescent reporter genes [e.g., red and green fluorescent proteins (RFP/GFP), respectively] and targeted fluorophors[15,16] [e.g., FITC fluorescin conjugated lectin]. Confocal and two-photon imaging methods have been applied to obtain some 3-D data, but these methods are limited to a few hundred micrometers depth from the imaging surface.[17,18]

Three-dimensional optical-computed-tomography (optical-CT) and optical-emission-computed-tomography (optical-ECT), when combined with optical clearing techniques, can yield high-contrast and high-resolution 3-D images of microvasculature and/or any fluorescent moiety. They represent powerful new techniques for investigating structural, functional, and genetic therapeutic responses and relationships.[19]

In previous work optical-CT has been developed in the context of high resolution 3-D dosimetry for verification of radiation therapy treatments.[20–23] Later, the technique was extended to include emission tomography, and applications were explored in developmental embryology and embryonic gene expression.[24,25] Recently, a novel implementation was presented[26] along with initial applications imaging xenograft tumors[27] and whole unsectioned rodent organs. In this paper, we review recent developments in optical-CT and optical-ECT techniques and compatible clearing protocols[28] and illustrate their application with an in-house benchtop imaging system (Fig. 1).

Address all correspondence to Mark Oldham, Radiation Oncology and Biomedical Engineering, Duke University Medical Center, Room 04216, Red Zone - Duke South Clinics, Durham, NC 27710; Tel: 919 668 0349; Fax: 919 681 7183; E-mail: mark.oldham@duke.edu

1083-3668/2008/13(2)/021113/8/$25.00 © 2008 SPIE

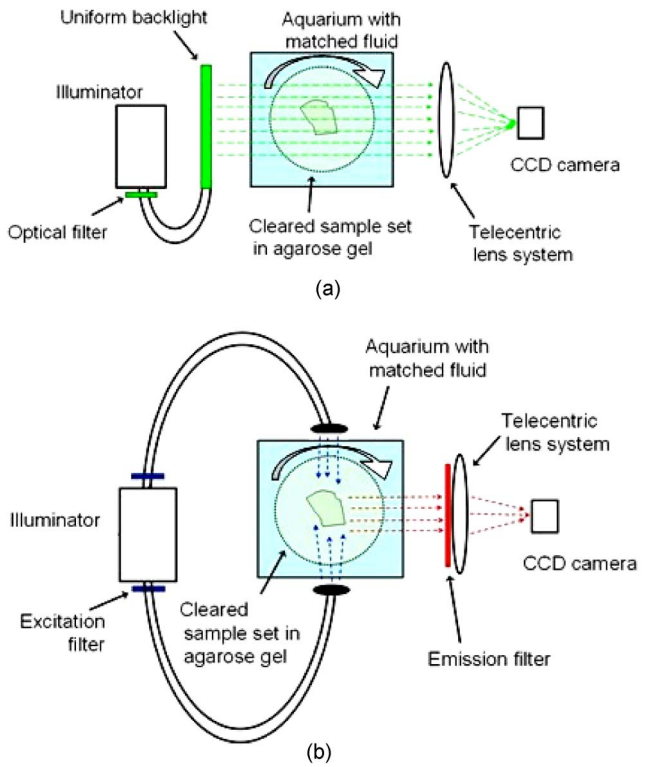

Fig. 1 Schematic of light paths through a prototype optical-CT (a) and optical-ECT (b) imaging system. In optical-CT, light from a uniform backlight traverses through the sample to form projection images captured by a CCD camera. In optical-ECT, incident light orthogonal to the imaging axis stimulates fluorescence in the sample. In both modes, a telecentric lens is used to form an image dominated by light parallel to the optic axis, thereby best approximating the parallel ray geometry and minimizing scatter contamination. (Based on Oldham et al.[26])

2 Basic Principles of the Optical-CT and Optical-ECT Techniques

Optical-CT can be conceived as the optical analog of x-ray CT. Three-dimensional images of the distribution of optical attenuation throughout a sample are reconstructed from optical projection images of light transmitted through the sample. Optical-ECT is the optical analog of SPECT (single-photon emission tomography). In optical-ECT, 3D images of the distribution of emitting light sources (e.g., fluorochromes) are reconstructed from emission images of light emitted from the sample. Some of the established benefits associated with combining image data from complimentary modalities, such as x-ray-CT/SPECT or x-ray-CT/PET (positron emission tomography), translate over to the optical-CT/optical-ECT combination. These include the facility for accurate registration of transmission and emission image data and the potential for relating tissue structure and function, as demonstrated here in relation to xenograft tumor imaging.

2.1 *Imaging Hardware and Acquisition*

Optical projection/emission images are acquired of a sample suspended in (for example) an agarose gel, mounted vertically on a rotating platform inside a small aquarium made from antireflection-coated glass. The gel rotates inside a high-refractive-index matched fluid, which minimizes refraction, enabling straight-line projection/emission images to be acquired. In optical-CT (transmission mode) light from a uniform back-light traverses through the sample to image formation at the CCD. Projections are acquired in a "step-and-image" manner at small angular increments (e.g., 0.3 deg) through a complete 360-deg revolution. In optical-ECT (emission mode) excitation light causes longer wavelength fluorescent light to be emitted within the sample, which is then also imaged on the CCD, as illustrated. The use of telecentric lenses in the optical imaging system facilitates accurate optical-CT and optical-ECT images, as image formation occurs from light traveling parallel to the optic axis. Acquisition proceeds in the same step-and-image procedure, with the same settings and constraints as already described. A key difference is that narrow-bandwidth optical filters are used to select both the excitation and emitting wavelengths. High-quality filters greatly enhance effective image quality by reducing any contaminant autofluorescence. A DSRed2 filter set was used to select for the excitation and emission wavelengths corresponding to RFP (558 and 583 nm, respectively). Exposure of the sample to excitation light was minimized by utilization of a shutter, which permitted exposure only during image acquisition. Consistent interprojection normalization was achieved by keeping the exposure time constant for each projection.

Once a complete set of projection or emission images has been acquired, 3-D reconstructions of the sample were created using the commercial COBRA Feldkamp filtered back-projection algorithm (Exxim Computing Corp, Pleasantown, California). Input parameters were adjusted to reflect the geometries of the image acquisition. In principle, the spatial resolution can approach the resolution of the CCD camera as the resolution of the lens is usually far higher. In practice, however, resolution is lost through the tomographic reconstruction and artifacts arising from motion point spread function and projection noise. Present prototype systems have been reported to have a modulation transfer function (MTF) $\sim$10% at 20 lp/mm, but substantial improvements are expected. The microoptical-CT scanner presented in Fig. 1 represents a second-generation and very fast scanning system when compared with the first-generation optical-CT devices described elsewhere.[20–22,29,30] The time for a typical acquisition of 360 projections was about 5 min.

2.2 *Optical Clearing for Optical-CT and Optical-ECT*

A significant difference between the optical and x-ray imaging analogs is that the poor optical transmission of biological tissue necessitates *ex vivo* sample preparation to improve optical transmission (the optical clearing process). Despite this limitation, accurate "*in vivo*" functional information is entirely feasible because optical stains and fluorescing labels can be applied *in vivo*, such that representative staining/labeling is achieved for subsequent imaging. Meaningful imaging of any functional parameter therefore requires preservation of the condition of that stain/label through the excision and sample preparation procedures. Optical clearing can be achieved by dehydration and reperfusion of the tissue with a transparent solution of high refractive index close to that of the cell nuclear and organelle membranes. In general, better-

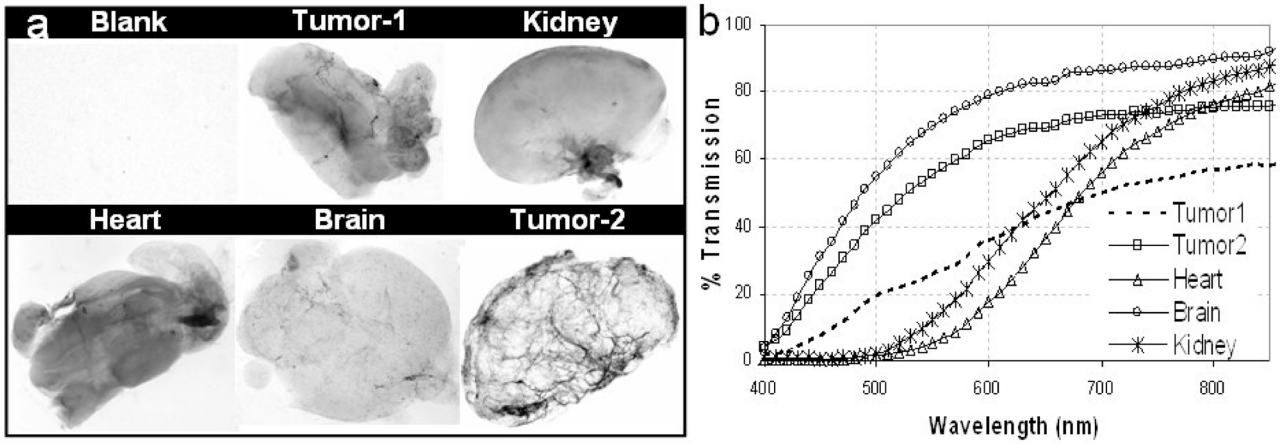

Fig. 2 (a) Light transmission projection images of a variety of optically cleared unsectioned tissue samples, acquired using the imaging system illustrated in Fig. 1(a), with a backlight of wavelength 633 nm and (b) light absorbtion characteristics of these samples acquired with a spectrophotometer, relative to pure methyl salicylate.

reconstructed image quality (both optical-CT and optical-ECT) is directly associated with better optical clearing, provided the signal of interest (here isotonic-ink in the vasculature, and fluorescent proteins) are not affected by the optical clearing process. Illustrative projection images through various unsectioned tissue samples that were cleared and labeled using the processes described later are shown in Fig. 2(a). The images were acquired using the system shown in Fig. 1(a), with a backlight source of wavelength 633 nm. Corresponding transmission characteristics of the samples relative to methyl-salicylate are shown in Fig. 2(b). All samples were imaged immersed in methyl salicylate. The lowest transmission was observed for the rat heart because of the high concentration of ink taken up in the vasculature and ventricle chambers. The highest transmission is observed in the brain, where ink uptake was greatly reduced due to the blood brain barrier.

2.2.1 *General sample preparation*

All samples were whole (i.e., unsectioned) at the time of imaging and optically cleared to enable visible light penetration through the sample. The principle of optical clearing is to replace the water-based cellular fluid with a solution of high refractive index to match that of the cell, nuclear, and organelle membranes.[31,32] Achieving quality optical clearing is a key step that enables the feasibility of both optical-CT and optical-ECT. All tissue samples imaged in this paper were first set in 0.75% agarose gel by weight. The tissue samples were positioned centrally and ~1 cm up from the bottom of the gel. Staining and fixing procedures varied between samples, and details are discussed in the corresponding following sections. The purpose of the agarose gel was to stabilize the sample during rotation incurred in the optical-CT/optical-ECT acquisition. Each sample (agarose and imbedded tissue) was then immersed in a succession of graded ethanol/water solutions, until the tissue was completely dehydrated. Once the sample was fully permeated with 100% ethanol, they were then immersed in a succession of graded ethanol with methyl-salicylate or benzyl-alcohol benzyl benzoate (BABBs), until the ethanol was completely replaced by the higher refractive index liquid. The large pore size of agarose gel facilitates efficient fluid exchange. Methyl salicylate was used for clearing any tissue sample containing fluorescent proteins, as better fluorescent preservation has been observed. For nonfluorescent samples, optical clearing was achieved with BABBs solution, which leads to slightly better optical clarity. These are the only clearing solutions we have tested so far but, in principle, any transparent solution with high refractive index (~1.54) that can be perfused into tissue can be a viable clearing agent. The solutions have negligible influence on the physical size and shape of organ. Furthermore, hematoxylin-and-eosin (H&E) histological evaluation of cleared specimens are virtually indistinguishable from control noncleared specimens. However, we have been unsuccessful so far in achieving immunohistological staining on tissue samples that have been optically cleared in this way.

2.2.2 *"Fluorescence-friendly" optical clearing*

Oldham et al.[27] investigated the feasibility of 3-D imaging the viable tumor burden in HCT116 tumor xenografts. The HCT116 cell line had been transfected with a gene coding for constitutively expressed[33] RFP. Viable tumor cells therefore express red fluorescence when exposed to the excitation wavelength. The initial challenge was to develop a tissue optical-clearing procedure that would preserve RFP fluorescence in the cleared tissue. A series of plating experiments were performed, where the transfected HCT116 tumor cells were exposed to a variety of tissue-fixing and clearing agents representing different potential clearing processes. Full details of the clearing procedures are given in Ref. 28. The effect on RFP and GFP fluorescence is shown in Fig. 3. The significant result from these experiments is that substantial fluorescence preservation was achieved when the initial cell fixation was in ethanol. Fixation in either PFA or methanol resulted in almost complete loss of fluorescence [Figs. 3(A) and 3(B)]. Furthermore, after ethanol fixation, the cells proved robust to subsequent exposure to either clearing agent BABBs or MetSal. To successfully image RFP in whole xeneograft tumors, the results of the plating experiments must be transferred to whole tumor specimens. This was achieved by first performing

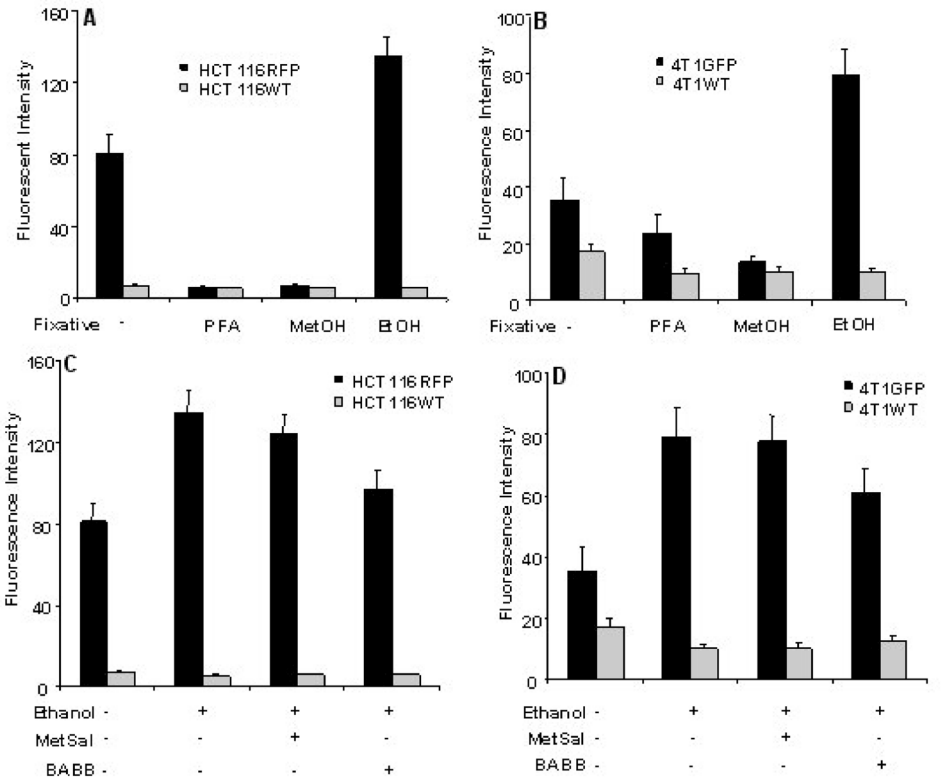

Fig. 3 Fluorescent light intensity from cells labeled with RFP and GFP, after exposure to various fixing and clearing solutions. Two cell lines were tested, human colon cancer (HCT116) and human breast cancer (4T1). Comparisons are shown against wild-type (WT) controls, which had no fluorescent labeling. (A) Effect of fixing agents on RFP intensity, (B) effect of fixing agents on GFP intensity, (C) effect of clearing agents on RFP, and (D) effect of clearing agents on GFP. (Based on Sakhalkar et al.[28])

perfusion-fixation of the tumors *in situ*, by aortic cannulation and gravitational drip feed of ethanol. Tumors were then placed in ethanol at 4°C overnight, and set in 0.75% agarose the next day. The clearing procedure involved perfusion graded solutions of water:ethanol, and then ethanol:methyl-salicylate. The total clearing process for tissue samples of order 1 cm^3 typically takes from 1 to 3 weeks, depending on size of sample, under gentle motion-assisted diffusion processes at room temperature. A similar procedure was used irrespective of the particular agent used for dehydration and clearing steps. The sample is initially placed in a 75:25 ethanol:water solution, which is changed to 100% ethanol after 12 h, and then refreshed on a daily basis for 4 days. Complete dehydration is necessary to avoid precipitation of opaque regions of agarose, which may occur if water and clearing agent react with agarose gel. The sample is then placed in a 50:50 solution of ethanol:clearing agent. After 24 h, the solution is changed to 100% clearing agent, which is also replenished on a daily basis.

3 Application of Optical-CT and Optical-ECT

3.1 *Imaging Xenograft Tumors*

Oldham et al.[27] presented preliminary data imaging HCT116RFP xenograft colon cancer tumors, containing constitutive RFP labeling, grown on the hind legs of nude mice, following the procedures of an Institutional Animal Care and Use Committee (IACUC) approved protocol. When the tumors had grown to a ~1 cm length, labeling/staining of the tumor microvasculature was achieved by tail vein injection and subsequent natural circulation around the body of a double bolus of isotonic india ink and fluorescent probe (lectin conjugated with FITC). The carbon-based ink particles circulate in the blood stream and are phagocytosed inside endothelial cells of the vessels, thereby marking patent microvasculature.[34] At 5 to 10 min postinfusion, the mouse was sacrificed and the tumor removed for sample preparation. Lectin actively binds to endothelial cells of the microvasculature, providing independent labeling of the microvasculature amenable for optical-ECT imaging. The implementation of both passive and active labeling of microvasculature enables cross-validation and comparison of both techniques. A single optical transmission or projection image of the whole HCT116 tumor is shown in Fig. 4(A), and contrasted with micro-x-ray-CT and micro-MRI images acquired with state of the art small animal imaging systems[35,36] [Figs. 4(B) and 4(C)] to highlight the excellent contrast and resolution of optical-CT. Exquisite visualization of the microvasculature was observed in the optical projection, although the 3-D nature of the vascular network is lost. In this instance, the vasculature is primarily seen on the periphery of the tumor, with a few larger vessels penetrating to the tumor core. As these tumors were implanted subcutaneously, especially dense and intensive vasculature is seen along one side of the tumor

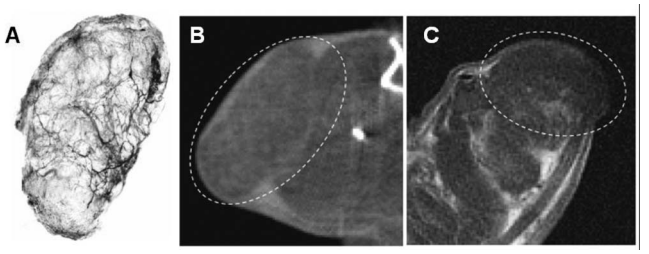

Fig. 4 (A) Projection image of the HCT116 tumor after optical clearing, (B) *In vivo* micro-CT of the same tumor on hind leg of mouse. The micro-CT image is reconstructed at 100-μm pixel resolution and involved application of a new vascular contrast agent (fenestra). (C) *in vivo* T1-weighted contrast-enhanced micro-MRI image of a similar tumor of same size acquired on the 2T system at the CIVM (Centre for Invivo Microscopy at Duke). MRI contrast was achieved with a continuous infusion of magnevist. The location of the tumor is indicated by the dashed line. (From Oldham et al.[27])

where it was attached to the underlying fascia of the animal.

Quantitative information is available from CT reconstructions of the projections. Figures 5(A)–5(C) show such a reconstruction from 240 projections acquired at 1.5-deg increments. The original projection images (1040×1388 pixels) were downsized to 748×998 (to match present software restrictions) and reconstructed on a $512\times512\times512$ grid. The pixel dimensions in the image are thus ~30 μm, although a greater number of projections must be acquired to meet the Nyquist criteria for this resolution limit. Significant vascular penetration is observed to be limited to the lower part of the tumor [Fig. 5(B)], indicating this region was relatively well perfused. The corresponding reconstructions of the emitting FITC distribution within the tumor, acquired with the FITC filters, are shown in Figs. 5(D)–5(F). In general, a clear correlation and agreement is observed between the optical-CT and optical-ECT images. Well-perfused regions appear bright in the optical-CT images (corresponding to regions high ink absorption) and also as bright regions in the optical-ECT images (where the scale is inverted such that light pixel values correspond to high emission of light and hence high concentration of FITC). The HCT116 tumor was also imaged in optical-ECT mode with DSRed2 filter set [Figs. 5(G) to 5(H)]. This image is significant as it represents the 3-D distribution of RFP emitted by viable tumor cells. The correlations between the corresponding views in Fig. 5 are striking, and clearly show that regions of high RFP expression correlate closely with the well-perfused regions. This makes intuitive sense, as one would expect the more viable regions of the tumor to correlate with perfusion. A precise interpretation is

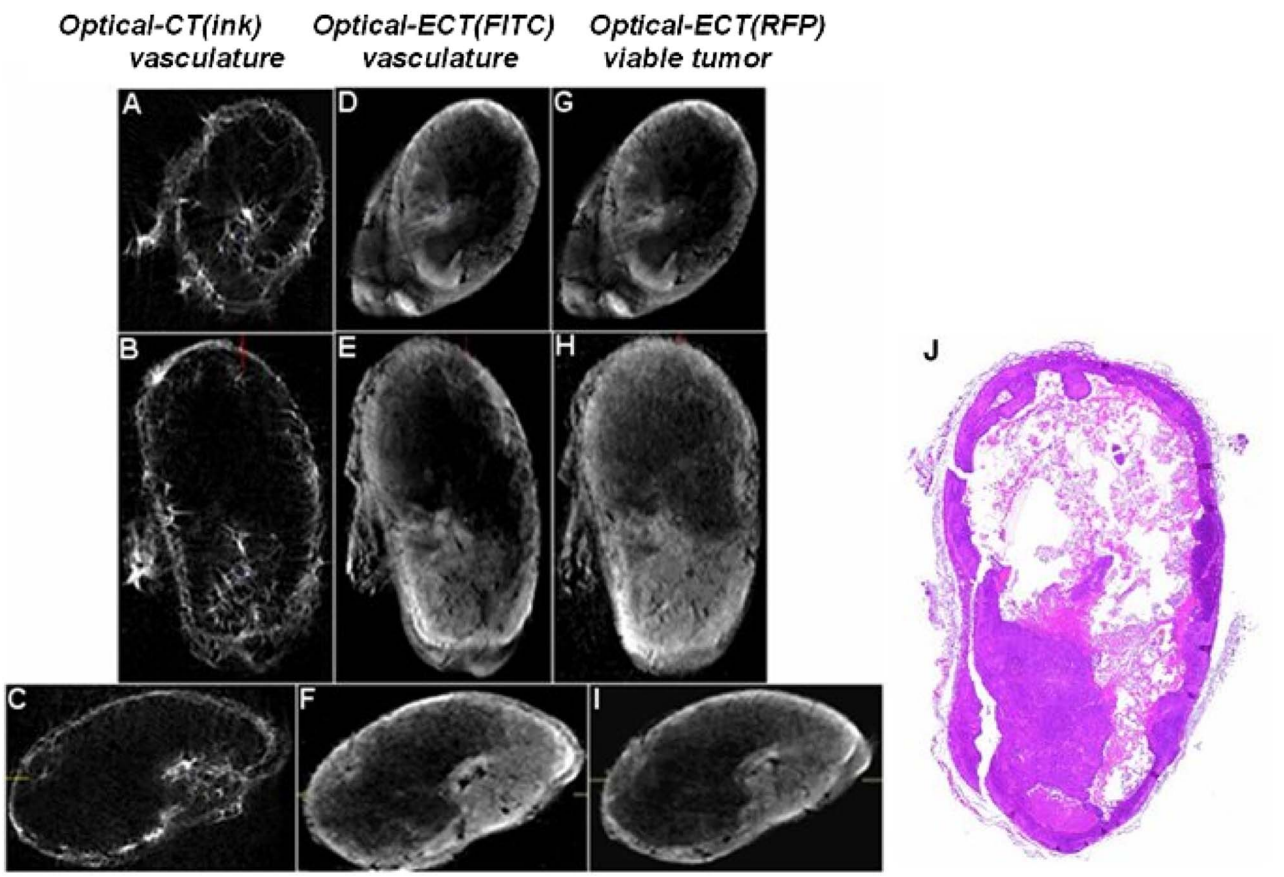

Fig. 5 (A) to (C) Orthogonal views of microvasculature of a HCT116 tumor stained with light-absorbing ink and imaged by optical-CT incorporating a white light source. Light regions of high perfusion are clearly visible as containing relatively high amounts of light attenuating ink. (D) to (F) microvasculature of a HCT116 tumor stained with FITC-conjugated lectin and imaged by optical-ECT incorporating the FITC excitation and emission filter set. (G) to (I) the distribution of viable tumor cells in the HCT116 tumor obtained by optical-ECT using the DSRed2 filter set to select for RFP excitation and emission. (J) conventional H&E stained histological section corresponding to views (B), (E), and (H).

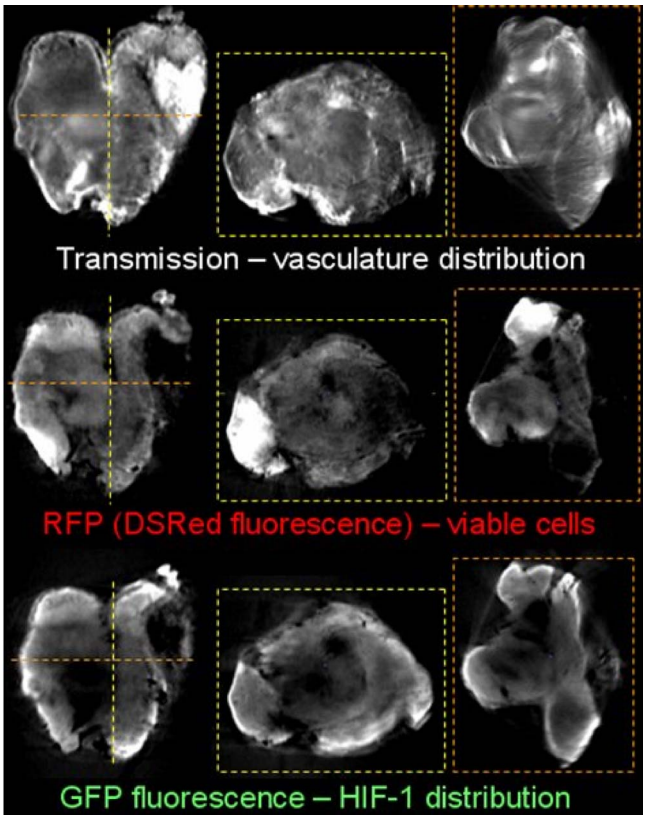

Fig. 6 Orthogonal views through 3-D reconstructions of HCT116 xenograft tumor imaged by optical-CT and optical-ECT. The tumors were triply labeled, with RFP and GFP flourescent reporter proteins, and light absorbing ink in the vasculature. Constitutive RFP labels the viable tumor burden, and GFP labeled HIF1 expression. The upper row is optical-CT images of vasculature. The middle row is optical-ECT images of the RFP (viable tumor) distribution. The lower row is optical-ECT images of the GFP (HIF1) distribution.

complex due to the novelty of these techniques, and requires reference to more established imaging modalities. Further interpretation of the optical-ECT images would require an attenuation correction, similar to that routinely encountered in SPECT imaging. Comparison with conventional histological sections [Fig. 5(J)] provided strong supporting evidence for the conclusions derived above from the optical imaging modalities. The peripheral band of well-perfused viable cells, inferred from all three optical reconstructions [Figs. 5(B), 5(E), and 5(H)] exhibits strong H&E staining in histological section (Fig. 5(J)) and therefore viable cells in this region. The large central areas devoid of vasculature and viable cells, as determined from the optical modalities, are indeed found to be devoid of H&E stain, indicating regions of necrosis.

The images shown in Fig. 5 were acquired with a prototype microscope-based optical system that incorporated nontelecentric optical components with limited suitability for tomographic imaging due primarily to limited depth of field. More recent images of similar tumors acquired with the bench system of Fig. 1 are shown in Fig. 6. A significant improvement in image quality is observed, through the removal of artifacts associated with the limited depth of field of the microscope system. Figure 6 also presents the first reconstructions of endogenous gene expression in three dimensions in xenograft tumors using optical-ECT. This was achieved using

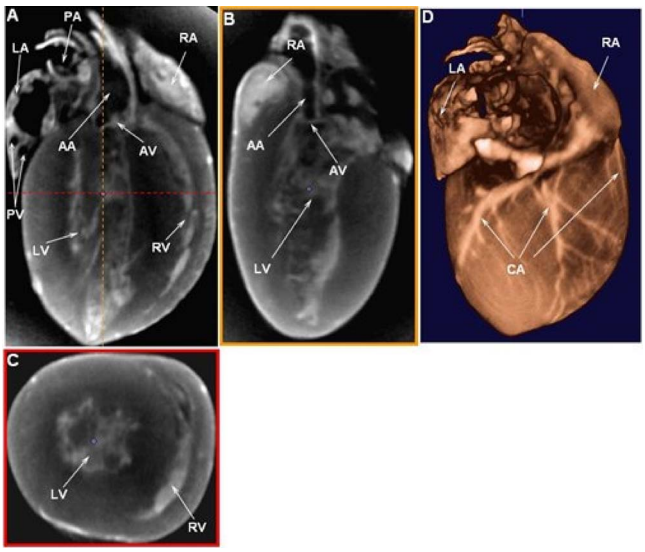

Fig. 7 Orthogonal views (A) to (C) through a 3-D optical-CT reconstruction of a normal rat heart and (D) a surface rendered image. Labels are LV/RV, right and left ventricles; AV, aortic valve; RA, right atrium; PA, pulmonary arch; AA, ascending aorta; PV, pulmonary veins; and CA, coronary arteries.

FITC filter sets and an HCT116 cell line that was double labeled with reporter proteins. Constitutive RFP-labeled viable tumor (as in the preceding), but secondary GFP labeling was incorporated to report the expression of the HIF1 gene.[33] While further work (for example, development of an attenuation correction for optical-ECT) and independent validation are required to fully understand the interpretation of these images, the potential utility is evident.

3.2 *Whole Rodent Organ Imaging*

Vascular staining in rodent organs was achieved by tail vein injection of isotonic ink as described in Sec. 3.1. Organs were prepared for optical-CT imaging using the procedure outlined in Sec. 2.1. Reconstructed images of a rat heart and lung are shown in Figs. 7 and 8, respectively. Postimaging histological

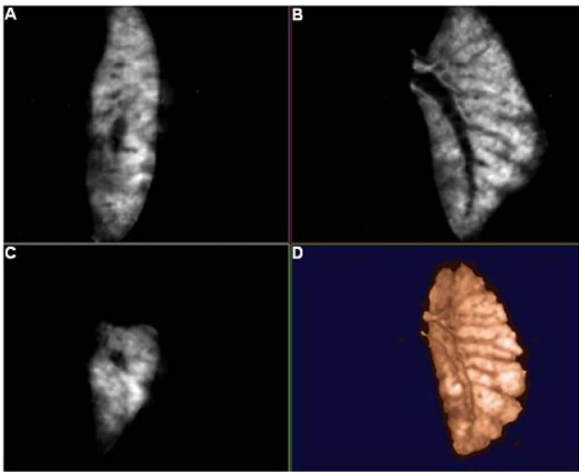

Fig. 8 (A) to (C) Orthogonal views through a 3-D optical-CT reconstruction of a normal rat lung and (D) surface rendered image.

study of these samples confirmed that the lighter regions in these images correspond to tissues with higher optical attenuation (greater ink staining), and higher perfusion.[26] In the heart images, the most prominent features are the coronary arteries, ventricles, and other areas of high blood content. Excellent detail of general heart structure is also observed. Similar observations are made in the lung images of Fig. 8. The major and minor bronchial airways are clearly visible, as are interesting variations in perfusion around the lung.

4 Discussion and Conclusions

Optical-CT and optical-ECT are relatively new imaging modalities that, when combined with optical clearing techniques, can provide unique 3-D information in high resolution and high contrast on the structure and function (including gene expression) of tissue. The optical clearing techniques reviewed here were developed from earlier techniques developed to clear thin sections of tissue for optical microscopy. A significant step forward was the development of clearing protocols that preserve the fluorescence output of unsectioned bulk tissue samples.[28] As with any new imaging modality, accurate interpretation of image content is gradually established by reference and correlation to alternative more established methodologies. The bulk of this effort has yet to be accomplished. Here, we reviewed the physical basis and demonstrated preliminary application to imaging xenograft tumor microvasculature and, for the first time, preliminary 3-D images showing endogenous gene expression in xenograft tumors (HIF1 expression), and whole rodent organs. The true potential of these techniques may be even wider, as it should be feasible to image a wide range of other tumor and normal tissue structures and functions, depending on the development of corresponding optical probes.

Acknowledgments

This work has arisen out of work funded by National Institutes of Health (NIH) Grant No. R01 CA 100835. The MR and microCT were performed at the Duke Center for In Vivo Microscopy an NCRR/NCI National Resource (P41 RR005959/R24 CA092656).

References

1. M. W. Dewhirst, R. Richardson, I. Cardenas-Navia, and Y. Cao, "The relationship between the tumor physiologic microenvironment and angiogenesis," *Hematol. Oncol. Clin. North Am.* **18**, 973–990 (2004).
2. R. K. Jain, "Antiangiogenic therapy for cancer: current and emerging concepts," *Oncology* **19**, 7–16 (2005).
3. P. Carmeliet and R. K. Jain, "Angiogenesis in cancer and other diseases," *Nature* **407**, 249–257 (Sep. 2000).
4. Y. Izumi, L. Xu, E. di Tomaso, D. Fukumura, and R. K. Jain, "Tumour biology: herceptin acts as an anti-angiogenic cocktail," *Nature* **416**, 279–280 (Mar. 2002).
5. P. Wachsberger, R. Burd, and A. P. Dicker, "Improving tumor response to radiotherapy by targeting angiogenesis signaling pathways," *Hematol. Oncol. Clin. North Am.* **18**, 1039–1057 (2004).
6. M. Garcia-Barros, F. Paris, C. Cordon-Cardo, D. Lyden, S. Rafii, A. Haimovitz-Friedman, Z. Fuks, and R. Kolesnick, "Tumor response to radiotherapy regulated by endothelial cell apoptosis," *Science* **300**, 1155–1159 (May 2003).
7. S. Shan, N. D. Robson, Y. Cao, T. Qiao, C. Y. Li, C. D. Kontos, M. Garcia-Blanco, and M. W. Dewhirst, "Responses of vascular endothelial cells to angiogenic signaling are important for tumor cell survival," *FASEB J.* **18**, 326–328 (2004).
8. R. K. Jain, "Antiangiogenic therapy for cancer: current and emerging concepts," *Oncology* **19**, 7–16 (2005).
9. B. J. Moeller, Y. Cao, Z. Vujaskovic, C. Y. Li, Z. A. Haroon, and M. W. Dewhirst, "The relationship between hypoxia and angiogenesis," *Semin. Radiat. Oncol.* **14**, 215–221 (2004).
10. B. J. Moeller, Y. Cao, C. Y. Li, and M. W. Dewhirst, "Radiation activates HIF-1 to regulate vascular radiosensitivity in tumors: role of reoxygenation, free radicals, and stress granules," *Cancer Cells* **5**, 429–441 (2004).
11. S. D. Barker, I. P. Dmitriev, D. M. Nettelbeck, B. Liu, A. A. Rivera, R. D. Alvarez, D. T. Curiel, and A. Hemminki, "Combined transcriptional and transductional targeting improves the specificity and efficacy of adenoviral gene delivery to ovarian carcinoma," *Gene Ther.* **10**, 1198–1204 (2003).
12. E. B. Brown, R. B. Campbell, Y. Tsuzuki, L. Xu, P. Carmeliet, D. Fukumura, and R. K. Jain, "In vivo measurement of gene expression, angiogenesis and physiological function in tumors using multiphoton laser scanning microscopy," *Nat. Med.* **7**, 864–868 (2001).
13. M. Wilke, E. Fortunati, M. van den Broek, A. T. Hoogeveen, and B. J. Scholte, "Efficacy of a peptide-based gene delivery system depends on mitotic activity," *Gene Ther.* **3**, 1133–1142 (1996).
14. K. L. Relph, K. J. Harrington, and H. Pandha, "Adenoviral strategies for the gene therapy of cancer," *Semin. Oncol.* **32**, 573–582 (2005).
15. C. H. Contag, D. Jenkins, P. R. Contag, and R. S. Negrin, "Use of reporter genes for optical measurements of neoplastic disease in vivo," *Aquacultural Eng.* **2**, 41–52 (2000).
16. R. Hoffman, "Green fluorescent protein imaging of tumour growth, metastasis, and angiogenesis in mouse models," *Lancet Oncol.* **3**, 546–556 (2002).
17. G. Alexandrakis, E. B. Brown, R. T. Tong, T. D. McKee, R. B. Campbell, Y. Boucher, and R. K. Jain, "Two-photon fluorescence correlation microscopy reveals the two-phase nature of transport in tumors," *Nat. Med.* **10**, 203–207 (2004).
18. T. W. Secomb, R. Hsu, E. Y. Park, and M. W. Dewhirst, "Green's function methods for analysis of oxygen delivery to tissue by microvascular networks," *Ann. Biomed. Eng.* **32**, 1519–1529 (2004).
19. M. Oldham, T. Oliver, and M. Dewhirst, "A novel method of imaging unperturbed tumor vasculature in 3D," *Int. J. Radiat. Oncol., Biol., Phys., Suppl.* **63**, S134 (2005).
20. M. Oldham, J. H. Siewerdsen, S. Kumar, J. Wong, and D. A. Jaffray, "Optical-CT gel-dosimetry I: basic investigations," *Med. Phys.* **30**, 623–634 (2003).
21. M. Oldham, J. H. Siewerdsen, A. Shetty, and D. A. Jaffray, "High resolution gel-dosimetry by optical-CT and MR scanning," *Med. Phys.* **28**, 1436–1445 (2001).
22. J. C. Gore, M. Ranade, M. J. Maryanski, and R. J. Schulz, "Radiation dose distributions in three dimensions from tomographic optical density scanning of polymer gels: I. Development of an optical scanner," *Phys. Med. Biol.* **41**, 2695–2704 (1996).
23. S. J. Doran, K. K. Koerkamp, M. A. Bero, P. Jenneson, E. J. Morton, and W. B. Gilboy, "A CCD-based optical-CT scanner for high-resolution 3D imaging of radiation dose distributions: equipment specifications, optical simulations and preliminary results," *Phys. Med. Biol.* **46**, 3191–3213 (2001).
24. J. Sharpe, "Optical projection tomography as a new tool for studying embryo anatomy," *J. Anat.* **202**, 175–181 (2003).
25. J. Sharpe, U. Ahlgren, P. Perry, B. Hill, A. Ross, J. Hecksher-Sorensen, R. Baldock, and D. Davidson, "Optical projection tomography as a tool for 3D microscopy and gene expression studies," *Science* **296**, 541–545 (Apr. 2002).
26. M. Oldham, H. Sakhalkar, Y. M. Wang, P. Guo, T. Oliver, R. Bentley, Z. Vujaskovic, and M. Dewhirst, "Three-dimensional imaging of whole rodent organs using optical computed and emission tomography," *J. Biomed. Opt.* **12**, 014009-1–014009-10 (2007).
27. M. Oldham, H. Sakhalkar, T. Oliver, Y. M. Wang, J. Kirpatrick, Y. Cao, C. Badea, G. A. Johnson, and M. Dewhirst, "Three-dimensional imaging of xenograft tumors using optical computed and emission tomography," *Med. Phys.* **33**, 3193–3202 (2006).
28. H. S. Sakhalkar, M. Dewhirst, T. Oliver, Y. Cao, and M. Oldham, "Functional imaging in bulk tissue specimens using optical emission tomography: fluorescence preservation during optical clearing," *Phys. Med. Biol.* **52**, 2035–2054 (Apr. 2007).
29. R. G. Kelly, K. J. Jordan, and J. J. Battista, "Optical-CT reconstruction of 3D dose distributions using the ferrous-benzoic-xylenol (FBX) gel dosimeter," *Med. Phys.* **25**, 1741–1750 (1998).

30. M. Oldham and L. Kim, "Optical-CT gel-dosimetry. II: Optical artifacts and geometrical distortion," *Med. Phys.* **31**, 1093–1104 (2004).
31. V. V. Tuchin "Optical clearing of tissues and blood using the immersion method," *J. Phys. D* **38**, 2497–2518 (2005).
32. F. Zhou, Y. He, and R. K. Wang, "A theoretical model on optical clearing of biological tissue with chemical active agents," in *Progress in Biomedical Optics and Imaging*, *Proc. SPIE* **5486**, 173–179 (2004).
33. Y. Cao, C. Y. Li, B. J. Moeller, D. Yu, Y. Zhao, M. R. Dreher, S. Shan, and M. W. Dewhirst, "Observation of incipient tumor angiogenesis that is independent of hypoxia and hypoxia inducible factor-1 activation," *Cancer Res.* **65**, 5498–5505 (July 2005).
34. D. E. Hilmas and E. L. Gillette, "Tumor microvasculature following fractionated x irradiation," *Radiology* **116**, 165–169 (1975).
35. C. Badea, L. W. Hedlund, and G. A. Johnson, "Micro-CT with respiratory and cardiac gating," *Med. Phys.* **31**, 3324–3329 (2004).
36. B. T. Chen, A. T. Yordanov, and G. A. Johnson, "Ventilation-synchronous magnetic resonance microscopy of pulmonary structure and ventilation in mice," *Magn. Reson. Med.* **53**, 69–75 (2005).